한국부식학회지
J. Corros. Sci. Soc. of Korea
Vol. 18, No. 1, March, 1989
〈研究論文〉

High Temperature Internal Oxidation Behavior of Iron Based Alloys

Jeong Y. Lee

Department of Materials Science, Korea Institute of Technology

A study of growth kinetics and microstructure of internal oxides in the iron-base alloys was carried out by an optical microscope and a scanning electron microscope, so that the growth mechanisms of the oxide precipitates in the internal oxidation zone could be understood in detail.

Iron-based alloys, Fe-1%Al, Fe-1%Al-1%Hf, Fe-1%Cr, Fe-1%Cr-1%Hf and Fe-2%Hf, were oxidized in a sealed quartz tube containing Fe/FeO powder mixtures which maintained the oxygen partial pressure at the FeO decomposition pressure at 800°C for the various time periods to 121 hours.

Results show that the growth rate of the oxide precipitates in the internal oxidation zone is controlled by the diffusion of oxygen. The variation of the solute element and the addition of Hf in the iron-base alloys led to a change in the depth of internal oxidation zone and in the oxide morphology. The internal precipitate adopted the form of continuous needles or feathers for the Fe-Al system, whereas that in the Fe-Cr and Fe-2%Hf systems adopted the form of discontinuous crystallites, that is, spheres or polyhedral crystallites. The mechanism of this morphological evolution was explained in detail.

1. INTRODUCTION

There are two essential requirements for high temperature oxidation resistant alloys. Firstly the diffusion through its oxide scale must be slow. Secondly this oxide scale must be adherent to the metal. Al_2O_3 and Cr_2O_3 scales fulfill the former requirement but the adherence to the metal is poor, particularly in case of thermal cycling condition. Previous researches[1),2),3),4),5)] have shown that the small addition of active element Hf in the alloy, significantly improved the adhesion of the scale to the metal. The formation of inwardly growing oxide pegs, which mechanically key the scale to the metal is known as a main factor for the scale adhesion.[3),4)] Mechanical keying of the

oxide to the alloy substrate, as a result of the internal oxidation of the active alloying addition, or dispersoid particles growing in size to form oxide stringers of thin elongated oxide intrusions extending into the alloy substrate, has been suggested by many authors (see ref. 2). Furthermore, the development of a peg-like morphology or a tortuous alloys/scale interface as a result of the internal oxidation is anticipated to improve scale adhesion for the following reasons:[6] (1) Relief of thermal as well as athermal stresses, arising from growth or differential dilatation/contraction, respectively. The intermediate, mixed alloy/oxide region would act as a graded seal, gradually accommodating the variation in physical properties of the two phases. (2) Impediment of crack propagation due to: (a) the obvious longer path; (b) large interfacial contact areas associated with extreme non-uniformities in peg microstructure; and (c) alloy hindrance since stress relief is achieved by plastic deformation of the alloy protrusions trapped between the pegs, rather than fracture of the brittle scale.

Internal oxidation under the external scale has a significant effect on the corrosion behavior of materials. The regular distribution of oxide protrusions is the most desirable in determining oxide/scale adherence. The inwardly growing oxide pegs which develop on subsequent exposure to oxidizing environments seem effective in keying the oxide surface scale to the substrate and thereby improving the oxidation resistant of this type of alloy under both isothermal and particularly thermal cycling condition. Thus, the internal oxide morphology has a significant effect on the adhesion of the scale to the metal. The aim of this research is to study the morphology and the growth kinetics of internal oxide precipitates.

2. EXPERIMENTAL PROCEDURE

The three binary alloys (Fe-1%Al, Fe-1%Cr, Fe-2%Hf), and two ternary alloys (Fe-1%Al-1%Hf, Fe-1%Cr-1%Hf) used for this work were prepared in an argon induction furnace. The reasons for the choice of the alloys (Table 1) were as follows: (1) The variation of the solute element and the addition of Hf were more effective in modifying the internal oxide morphology than the variation of the solute content. Increasing the solute content led to an increase in the internal oxide size and volume fraction. (2) The free energy of formation for Al_2O_3, Cr_2O_3, and HfO_2 is much more negative than that of FeO. So the element Al, Cr, Hf can form the internal oxide in the alloy.

Table 1. Alloy compositions (weight %).

Alloy	Fe	Al	Cr	Hf
Fe-1%Al	99	1	0	0
Fe-1%Al-1%Hf	98	1	0	1
Fe-1%Cr	99	0	1	0
Fe-1%Cr-1%Hf	98	0	1	1
Fe-2%Hf	98	0	0	2

The 99.99% pure iron, aluminum and chromium pellets, and 99.999% pure hafnium powder were weighted, combined, and heated to 1500°C. The melts were held at this temperature for fifteen minutes to insure complete mixing, and pured into cylindrical molds of 3X28 cm. All the alloys listed above were cut in small rectangular sample of 15X10X3 mm. In order to achieve similar oxidation conditions,

the samples were metallographically polished with SiC abrasive papers down to 30 μm grit size and finally ultrasonically cleaned in distilled water. During this stage, care had to be t 'en in order to prevent rusting to occur. This particular problem was encountered with the chromium specimens. The specimens must be swabbed with ethyl alcohol impregnated piece of cotton.

The specimens were hung on a small mullite rod through a hole drilled in them, and allowed to rest in the groove cut in the quartz boat. Several specimens rested on each small rod. Here, care was taken to prevent the specimen from sliding and coming in close contact. Some plaster was used in the middle of the rod for that purpose. The boat which was exactly 75 mm long was inserted all the way to the end of the tube. A 50/50 FeO/Fe mixture was inserted in three small crucibles and pushed until contact was made inside the reaction tube with the quartz boat. The quartz reaction tube was evacuated and back-filled with argon gas. Such a vacuum degree was under 1 mm of mercury of about 10^{-3} atm before backfilling with argon gas. The evacuation and back-filling procedure was repeated three times to minimize the residual oxygen and nitrogen gas in the reaction tube. The vacuum valve of the reaction tube was closed after back-filling and the tube removed from vacuum system was inserted inside the furnace. For internal oxidation without external scale, the oxygen partial pressure in the environment must be greater than that required to oxidize the alloying element but less than required to form FeO. Thus, the specimens were oxidized in the sealed quartz tube containing Fe/FeO powder mixtures which maintained the oxygen partial pressure at the FeO decomposition pressure at 800°C for the various time periods to 121 hours.

The reaction time was taken as that between the moment when the tube was fully inserted inside the furnace and when it was fully out. Five to ten minutes were necessary to either insert or remove the reaction tube from the furnace. Once the tube was outside the furnace, it was allowed to cool to room temperature. The samples were mounted in epoxy resin mounts properly labeled and polished for microscopic observation. The zone of internal oxidation was measured on conventionally-prepared metallographic cross sections using an optical microscope. The specimen for optical microscopic observation was etched with 1% nital solution. The specimens were deeply-etched by partial selective alloy dissolution in a 10% bromine-methyl alochol solution at 40°C for five minutes, technique devised to examine the morphology of internal oxide precipitates. These specimens were subsequently gold plated for observation under a scanning electron microscope.

The determination of the composition of the oxide precipitate within the internal oxidation zone was based on energy dispersive x-ray microanalysis and x-ray diffraction analysis. To minimize interference from the substrate, the measurements were performed on deeply-etched specimens.

3. RESULTS AND DISCUSSION

3.1 Growth Kinetics

All the specimens did not show any visible external scale, but showed "metallic" surface. The

surface was composed of "mirror like" plates of different reflectance. As mentioned in the procedure section each specimen was viewed in an optical microscope to determine the depth of internal oxidation, which is the distance from the alloy/gas interface to the deepest precipitate in the alloy. This distance was then averaged with other measurements.

Figure 1 shows the relationship between the depth of internal oxidation and the reaction time for the five alloys at 800°C. The plot has been made with the assumption of the parabolic rate law by plotting $\bar{x}$, the depth of the zone of internal oxidation, versus the square root of time, $t^{1/2}$. A straight line is then forced through the points defined for each sample by the least square method. The Fe-1%Cr-1%Hf alloys has the best data. The Fe-1%Al, Fe-1%Cr and Fe-1%Al-1%Hf alloys are less good. It can be noted that the greatest slope, that is, $x/t^{1/2}$ is obtained with Fe-2%Hf alloy and the smallest with Fe-1%Al alloy. But the differences in penetration among the alloys are slight. The difference becomes greater with increasing time

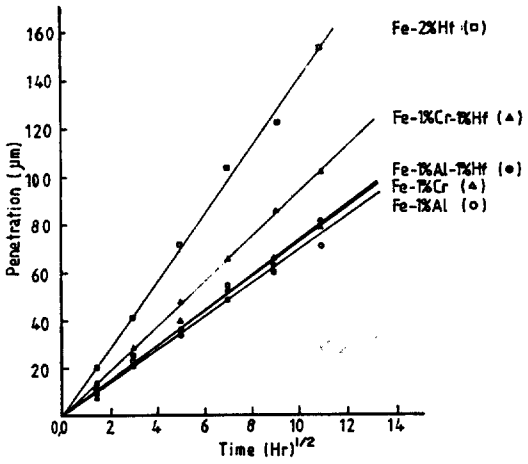

Fig. 1. Dependence of internal oxide growth rate on time of the five iron base alloys.

of treatment for Fe-1%Cr-1%Hf and Fe-2%Hf alloys.

It is evident that the addition of Hf to Fe-1%Al did not affect the growth rate significantly. But the addition of Hf to Fe-1%Cr significantly affected the growth rate. It is known that the small addition of Hf reduces the overall oxidation rate.[7] However, the growth rate of the internal oxidation zone was slightly increased with adding Hf in Fig. 1. The reason for this increased growth rate is presumably due to enhanced oxygen diffusion along the supposedly incoherent interface between the HfO_2 oxide particles, existing ahead of the oxide precipitate front, and the alloy matrix.[3),4)]

According to the analysis of Wagner,[9] if the kinetics of the reaction are diffusion controlled, the depth of the internal oxidation zone, $\bar{x}$, varies linearly with the square root of time.

$$\bar{x} = 2\gamma(D_O t)^{1/2} \quad (1)$$

where D_O is the diffusivity of oxygen in the base metal and γ is a dimensionless parameter, or in another form,

$$\bar{x} = kt^{1/2} \quad (2)$$

where k is the parabolic rate constant for the advance of the internal oxidation zone. We have $\bar{x} = kt^{1/2}$ equation which predicts a straight line passing through the origin for a plot of $\bar{x}$ versus $t^{1/2}$ as shown in Fig. 1. The advance of the precipitation zone is thus, approximately, described by a parabolic relationship in all cases. It is clear that the growth rate of the precipitate zone is controlled by the diffusion of oxygen in these iron-base alloys.

3.2 Microstructure

Figure 2 shows a typical cross-section optical micrograph of oxidized Fe-1%Al sample at 800°C for 121 hours. The internal oxidation zone is uniform as shown in this figure. They do not show any visible external scale in the micrographs. The oxide precipitates in the immediate vicinity of the surface are fine and dispersed. As one moves away from the surface, preferential precipitation along grain boundaries occurs. Between these grain boundary precipitates, the oxide particles assume a needle-like shape with a directional habit. All needle-shaped particles were oriented 30°–40° away from the normal of the original sample surface as shown in the micrograph. The oxide precipitates in the internal oxidation zone are shown in a scanning electron micrograph of Fig. 3. The sample was oxidized at 800°C for 121 hours and then deeply etched in a solution of 10% bromine and methyl alcohol to reveal the oxide precipitates. The penetration depth is uniform and 75 μm deep in this sample. It shows many needle-like precipitates in the internal oxidation zone. Note that most oxide precipitates are

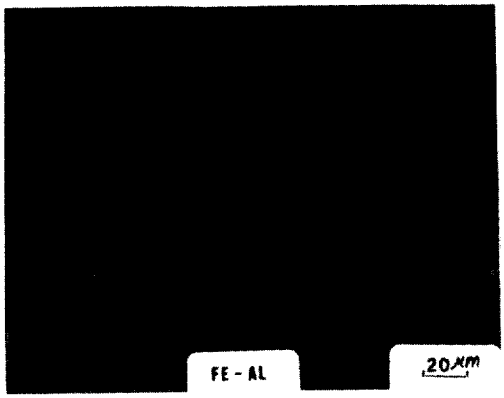

Fig. 2. Cross-section optical micrograph of the Fe-1%Al alloy oxidized at 800℃ for 121 hr.

Fig. 3. Cross-section scanning electron micrograph of the Fe-1% Al alloy oxidized at 800℃ for 121 hr showing the internal oxide morphology.

tilted 30°–40° away from the normal of the original alloy surface, and aligned nearly parallel to these directions, which indicate a directional habit of the precipitate. Also note that there are some oxide precipitates which are not continuous from the surface to the penetration depth because these oxide precipitates were cut away during polishing the sample. The compositio of the oxide particles within the internal oxidation zone was identified as Al_2O_3, based on energy dispersive x-ray analysis and x-ray diffraction analysis. Al K_α x-ray map for the needle-like precipitates in the Fe-1%Al alloy is shown on the right and the corresponding scanning electron micrograph on the left in Fig. 4.

Figure 5 shows a typical optical micrograph of oxidized Fe-1%Al-1%Hf sample at 800°C for 121 hours. The precipitates are very fine and uniform. The oxide precipitates show more fine needle-like shape than those in the Fe-1%Al in the optical micrographs. However, in a scanning electron micrograph as shown in Fig. 6, in contrast to the needle-like precipitate formed in the pure Fe-1%Al alloy, the addition

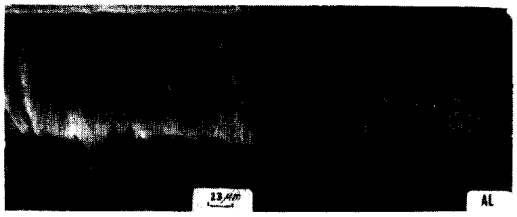

Fig. 4. Al x-ray map of the precipitation zone on the right and corresponding scanning electron microscopy image on the left.

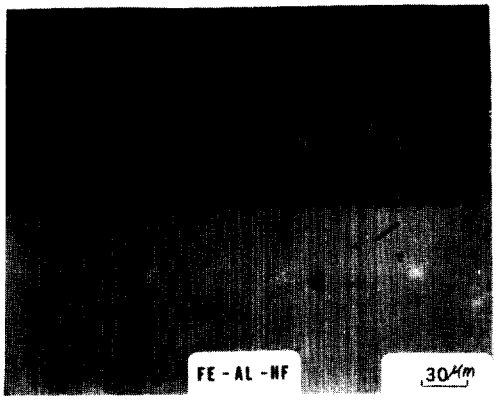

Fig. 5. Cross-section optical micrograph of the Fe-1 %Al-1 %Hf alloy oxidized at 800℃ for 121 hr.

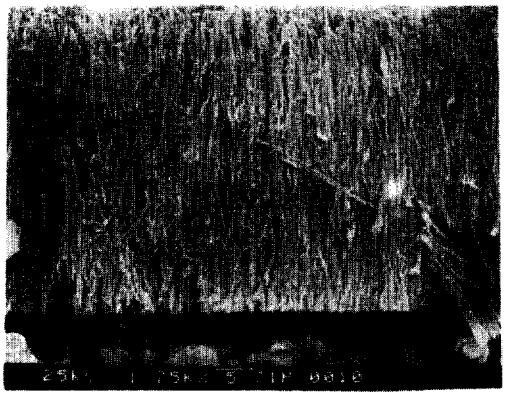

Fig. 6. Cross-section scanning electron micrograph of the Fe-1 %Al-1 %Hf alloy oxidized at 800℃ for 121 hr showing the internal oxide morphology.

of Hf led to a marked morphological change. The addition of the active element Hf made the oxide precipitates more fine and disperse. The oxide particles in the Hf containing alloy exhibited a feather-like morphology with several branches rather than a needle-like shape in Fig. 6. Furthermore, the oxide precipitates are oriented nearly perpendicularly to the original alloy surface whereas the oxide precipitates in the Fe-1%Al alloy grow to 30°–40° tilted directions from the normal of the surface. Al K_α x-ray map for the oxide precipitates in the Fe-1%Al-1%Hf alloy is shown on the right and the corresponding scanning electron micrograph on the left in Fig. 7. The composition of the oxide precipitates within the internal oxidation zone was also identified as Al_2O_3.

Fig. 7. Al x-ray map of the precipitation zone in the Fe-1 %Al-1 %Hf alloy on the right and corresponding scanning electron microscopy image on the left.

Figure 8 shows a cross-section optical micrograph of the Fe-1%Cr alloy oxidized at 800°C for 121 hours. The oxide precipitates are fine near the surface, but grow bigger as they move from the surface. The particle size is nearly constant beyond a thin surface layer. The morphology of the oxide precipitates is clearly shown in a scanning electron micrograph of the internal oxidation zone in Fig. 9. The oxide precipitates, which were observed as

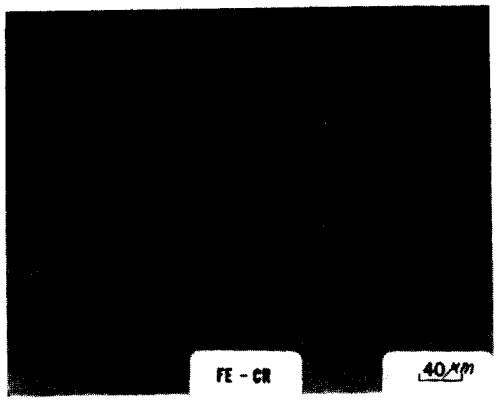

Fig. 8. Cross-section optical micrograph of the Fe-1 %Cr alloy oxidized at 800℃ for 121 hr.

Fig. 9. Cross-section scanning electron micrograph of the Fe-1 %Cr alloy oxidized at 800℃ for 121 hr showing polyhedral crystallites and grain boundary.

spherical crystallites in the optical micrograph, were observed as polyhedral crystallites in the scanning electron micrographs. Polyhedral crystallites are fine in the vicinity of the surface, but grow bigger as one moves away from the surface. The composition of the oxide particles within the internal oxidation zone was Cr_2O_3, based on energy dispersive x-ray analysis and x-ray diffraction analysis. Cr K_α x-ray map for polyhedral precipitates in the Fe-1%Cr alloy is shown on the right and the corresponding scanning electron micrograph on the left in Fig. 10.

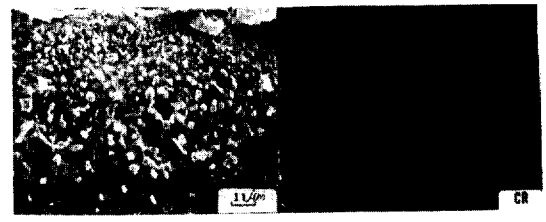

Fig. 10. Cr x-ray map of the precipitation zone on the right and corresponding scanning electron microscopy image on the left.

The addition of Hf to the Fe-1%Cr alloy did not lead to a significant morphological change, but reduced the oxide particle size as shown in Fig. 11. In a scanning electron micrograph of Fig. 12, the particle size of the precipitated oxide increases with the distance from the surface. Figure 13 shows a cross section optical micrograph of the Fe-2%Hf sample which was oxidized for 121 hours, and a scanning electron micrograph of the Fe-2%Hf sample which was oxidized at the same condition is shown in Fig. 14 In these figures, the precipitates are very

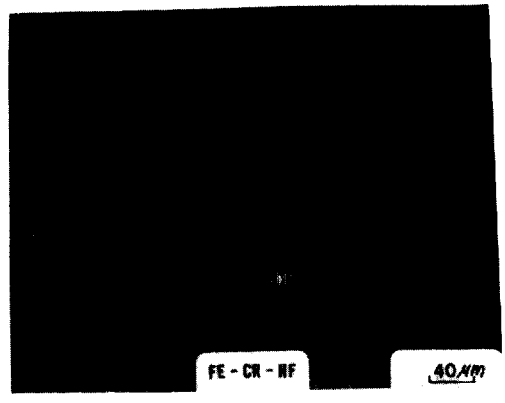

Fig. 11. Cross-section optical micrograph of the Fe-1 %Cr-1 %Hf alloy oxidized at 800℃ for 121 hr.

fine and dispersed. The particle size of oxide precipitates also increases with the depth.

For the Fe-1%Al and Fe-1%Al-1%Hf alloys, the internal precipitate always adopted the form of continuous needles or feathers extending virtually completely right the way through the internal oxide zone. The reason for this is presumably related to the degree of supersaturation existing ahead of the precipitate zone. It was suggested[10] that oxygen diffuses ahead of the precipitate zone causing the concentration product to exceed its equilibrium value at a finite distance ahead of the precipitate front. Eventually, it becomes high enough to provide sufficient driving force to nucleate a new oxide particle. It can be assumed that because of the high stability of Al_2O_3 there is never sufficient oxygen diffusing ahead of the precipitation zone to produce significant supersaturation of the matrix with respect to oxide. Thus the precipitate will continue to grow instead of nucleating a new oxide particle and the internal precipitate will adopt the form of continuous needles or feathers as shown in Figs. 3 and 5. However, if oxygen diffuses ahead of the precipitate zone causing the concentration product to exceed its equilibrium value at a finite distance ahead of the precipitate front, then, it becomes high enough to provide sufficient driving force to nucleate a new oxide particle. The oxide precipitate will adopt the form of discontinuous crystallites, that is, spheres or polyhedral crystallites as shown in Figs. 9, 12, and 14.

For the case of diffusion controlled precipitate growth, the average precipitate spacing is approximated by the distance between two successive point of nuclei formation,[10] i.e.,

Fig. 12. Cross-section scanning electron micrograph of the Fe-1 %Cr%-Hf alloy oxidized at 800℃ for 121 hr showing the internal oxide morphology.

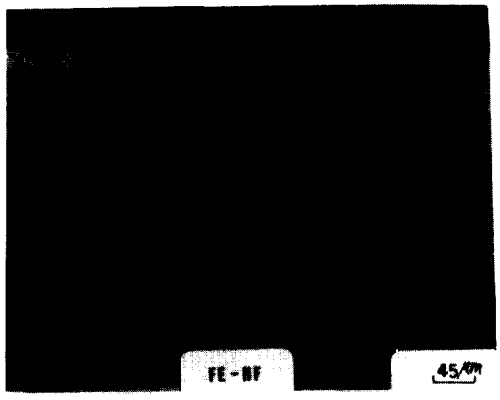

Fig. 13. Cross-section optical micrograph of the Fe-2 %Hf alloy oxidized at 800℃ for 121 hr

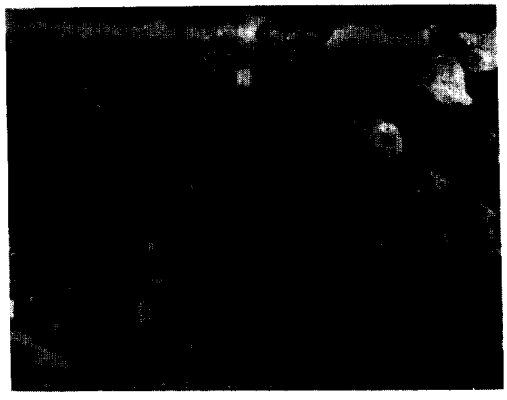

Fig. 14. Cross-section scanning electron micrograph of the Fe-2 %Hf alloy oxidized at 800℃ for 121 hr showing the internal oxide morphology.

$\Delta X = X'-X$. Then the number of precipitates $z(X)$ per unit volume may be given by the expression:

$$z(X) = (\Delta X)^{-3} = (\frac{X}{\Delta X})\frac{1}{X^3}. \quad (3)$$

To evaluate $z(X)$ in terms of the unknown parameters, N_O, N_B, N^*_O, and N^*_B, where N_O and N_B are the mole fractions of oxygen and solute B in the base metal, and N^*_O and N^*_B are the mole fractions of oxygen and solute B in the base metal critical to the formation of a nucleus of critical size, Bohm and Kahlweit solved simultaneously four equations involving these four unknowns and X/ΔX. This allows Equation (3) to be written as[11]

$$z(X) = \beta \frac{(N_O^{(s)})^3}{X^3} \quad (4)$$

where

$$\beta = \frac{1}{N_O^{(s)}} \frac{X}{\Delta X}$$

and $N_O^{(s)}$ is the mole fraction of oxygen at the external surface. Equation (4) allows two important quantities to be predicted. The first is that the number of precipitates per unit volume, depends inversely on the cube of the distance from the alloy/gas interface to the precipitate for a given $N_O^{(s)}$. The second is, that the number of the precipitates per unit volume at a given, X, will vary directly with the cube of the mole fraction of the oxygen at the alloy/gas interface. This fact is clearly shown in Figs. 9, 12, and 14 where the number of precipitates reduces rapidly with the distance from the alloy/gas interface to the precipitate.

For the situation, that of negligible solute enrichment into the internally oxidized zone, the radius, $r(X)$ of the spherical precipitates may be expressed as:

$$r(X) = (\frac{3V_{BO}N_B}{4\pi\beta})^{1/3} \frac{X}{N_O^{(s)}} \quad (5)$$

where V_{BO} is the molar volume of the oxide. However, this equation becomes invalid for either oxygen-solute atom clusters or for precipitates which are not spherical in nature. Note that the size of the precipitates, $r(X)$ depends on the distance, X, from the alloy/gas interface to the precipitate. For the Fe-1%Cr, Fe-1%Cr-1%Hf and Fe-2%Hf alloys, the particle size of the precipitated oxide increases with the distance from the surface as shown in Figs. 9, 12, and 14, which is consistent with Equation (5).

4. CONCLUSIONS

Iron-based alloys, Fe-1%Al, Fe-1%Al-1%Hf, Fe-1%Cr, Fe-1%Cr-1%Hf and Fe-2%Hf, were oxidized in a sealed quartz tube containing Fe/FeO powder mixtures which maintained the oxygen partial pressure at the FeO decomposition pressure at 800°C for the various time periods to 121 hours.

A study of growth kinetics and microstructure of internal oxides in the iron-base alloys was carried out by an optical microscope and a scanning electron microscope, so that the growth mechanisms of the oxide precipitates in the internal oxidation zone could be understood in detail.

The following results have been obtained:

1) The growth rate of the oxide precipitates in the internal oxidation zone is controlled by the diffusion of oxygen in these iron-base alloys, and the depth of the internal oxida-

tion zone varies linearly with the square root of time.

2) The small addition of Hf slightly increases the oxide growth rate in the internal oxidation zone.

3) For the Fe-1%Al alloy, the oxide precipitates show a needle-like shape with a directional habit. The addition of the active element Hf makes the oxide precipitates a fine feather-like shape with several branches, which grow perpendicularly to the original surface.

4) For the Fe-1%Cr alloy, the oxide precipitates are polyhedral crystallites which grow bigger as they move away from the surface. The addition of Hf to the Fe-1%Cr alloy reduces the oxide particle size.

5) For the Fe-2%Hf alloy, the oxide precipitates are very fine spherical crystallites.

REFERENCES

1. J.K. Tien and F.S. Pettit, *Met, Trans.*, **3**, 1587 (1972).
2. D.P. Whittle and J. Stringer, *Phil. Trans. Roy. Soc., London*, **A295**, 309 (1980).
3. I.M. Allam, D.P. Whittle and J. Stringer, *Oxid. Met.*, **13**, 381 (1974).
4. H. Hindam and D.P. Whittle, *J. Electrochem. Soc.*, **129**, 129 (1982).
5. R.A. Rapp, *Corrosion*, **21**, 382 (1965).
6. H. Hindam and D.P. Whittle, *Proc. of JIM Third International Symposium on High Temperature Corrosion of Metals*, Tokyo, Japan, Nov. 17-20, 1982.
7. D.P. Whittle and D.H. Boone, *Proc. of 7th LBL/MMRD International Materials Symposium, Surfaces and Interfaces in Ceramic and Ceramic-Metal System*, Lawrence Berkeley Laboratory, University of California, Berkeley, CA, Jul. 28-30, 1980.
8. D.P. Whittle, Y. Shida, G.C. Wood, F.H. Stott, and B.D. Bastow, *Lawrence Berkeley Laboratory Report*, LBL-13521, Lawrence Berkeley Laboratory, University of California, Berkeley, CA, Oct., 1981.
9. C. Wagner, *Z. Electrochem.*, **63**, 772 (1959).
10. G. Bohm and M. Kahlweit, *Acta Met.*, **12**, 641 (1964).
11. R.A. Rapp, *Proc. of 21st Conf. National Association of Corrosion Engineers*, St. Louis, Mo., Mar. 15-19, 1965.